IJE TRANSACTIONS C: Aspects Vol. 26, No. 12, (December 2013) 1525-1534

International Journal of Engineering

Journal Homepage: www.ije.ir

Numerical and Analytical Investigation in Radiated Noise by a Shock-Absorber

K. Mehraby[a], H. Beheshti[b], M. Poursina[b*]

[a] *Department of Mechanical Engineering, University of Shahrekord, Sharekord, Iran*
[b] *Department of Mechanical Engineering, University of Isfahan, Isfahan, Iran*

PAPER INFO

Paper history:
Received 07 October 2012
Accepted in revised form 16 May 2013

Keywords:
Noise
Impact
Shock-Absorber
Acoustics

ABSTRACT

In this article, the radiated noise by a shock-absorber is studied. This particular shock-absorber is used in a heavy-gauge shearing line in order to stop the cut steel sheets. Three steps are followed to evaluate the propagated sound in the surroundings; first of all, the plate vibration response is specified after the impact. Secondly, the edges of the plate are substituted by a set of the monopoles to model the effects of the edges in the sound generation. Thirdly, the Rayleigh integral equation is used to calculate the sound generated by the surfaces of the plate. The finite element method is also employed to simulate the problem.

doi: *10.5829/idosi.ije.2013.26.12c.13*

1. INTRODUCTION

Impact is an interesting field that ever attracts probers, particularly, when the impact is studied to realize an acoustic phenomenon. Some of the probers concentrated on massive bodies such as sphere [1, 2], cylinder, cone [3], or drop hammer [4]. Other probers studied other bodies such as beams [5] or plates. Plates are common elements in industrial machines that make intensive noise. Therefore, several manuscripts exist on noise radiated by the plates. Wahlin et al [6] photographed the sound waves around the impacted clamped plate. Schedin et al [7] studied the clamped plate by boundary element method. Moreover, there are some manuscripts [8-12] that survey baffled plates. Here, the radiated noise by steel sheets collided by a shock-absorber is studied. Shock-absorbers are very common mechanisms used in diverse industries. These mechanisms are used in stopping different bodies. These bodies can be massive or have extended surfaces. If a massive body is impacted, sound is generated by the rigid body acceleration. These kinds of bodies and sound generation by them are even studied in some manuscripts. The focus of this article is on a body with an extended surface. Here, the modal vibration as well as the rigid body motion affects the sound generation. The steel sheet shock-absorbers in heavy-gauge shear lines are an intensive source of sound pollution where modal vibrations have an effective role in the sound generation. In heavy-gauge shear lines plates are cut in different sizes. The sheets are conveyed to a piler. In the piler the sheets collide with a shock-absorber and are laid off. The dimensions of sheets can be different based on consumer order. Figures 1 and 2 show schemas of a heavy-gauge shear line and stopping mechanism, respectively.

The purpose of this article is to propose a method for acoustical optimization of the shock-absorbers. Hence, the noise radiated by collided sheets is studied. The vibrational response of the plate due to impact is specified in section 2. To specify radiated sound, the plates are partitioned into edges and the surfaces of the plates. The sound generated by the edges is predicted by utilizing the monopole formulation. It is supposed that the surfaces of the plates are extremely extended. Therefore, sound radiated by the surfaces can be predicted by Rayleigh integral equation. Finally, the total sound is calculated by summation of the sound generated by each part based on superposition law.

The finite element method (FEM) helps to find out more about sound generation and sound propagation. The following two steps are pursued to simulate the problem by FEM: the plate is exited by a half-sine impact force where the plate reactions are studied, and

*Corresponding Author Email: poursina@eng.ui.ac.ir (M. Poursina)

the state variables which were produced in the previous step are applied to excite the air elements. The excitation is applied based on the continuity law. Reactions of excited air elements can estimate the sound field.

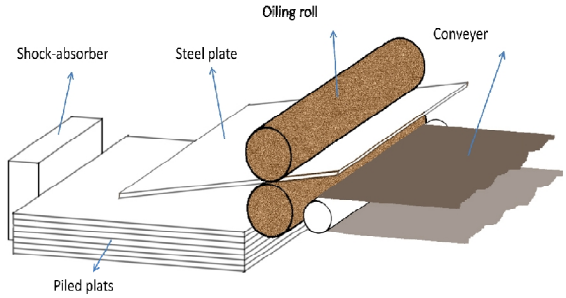

Figure 2. Scheme of stopping mechanism

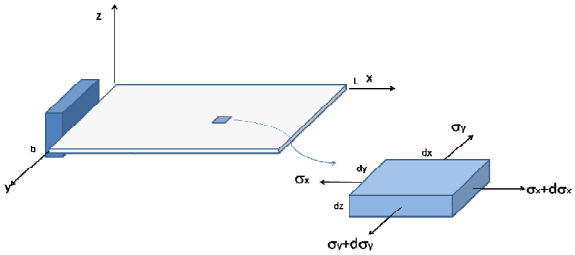

Figure 3. An element of the plate

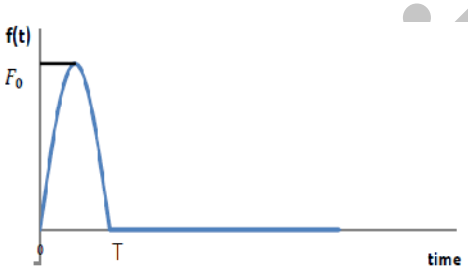

Figure 4. Behavior of contact force

2. VIBRATIONAL RESPONSE OF THE PLATE

Here, the modal analysis is used to specify response of the plate after the impact. It is assumed that the plate is absolutely suspended in the air through the collision due to the following reasons. First of all, the stopping mechanism shown in Figure 2 justifies this fact. Secondly, the core purpose of this study is not to deliberate the effects of boundary conditions in sound generation. The motion equation in x-direction for element shown in Figure 3 is written as:

$$(\sigma_x + d\sigma_x)\, dy\, dz - \sigma_x\, dy\, dz + f_x(x,y,z,t)\, dx\, dy\, dz - \rho\, dx\, dy\, dz\, \frac{\partial^2 u}{\partial t^2} = 0 \quad (1)$$

where, σ_x is the stress in x-direction, ρ is the density of the plates, t is the time, u is the deformation of the elements in x-direction, and $f_x(x,y,z,t)$ is the body force in x-direction. This equation, after simplification can be written as:

$$\frac{\partial \sigma_x}{\partial x} + f_x(x,y,z,t) = \rho \frac{\partial^2 u}{\partial t^2} \quad (2)$$

Similarly, the equation of motion in y-direction can be written as:

$$\frac{\partial \sigma_y}{\partial x} + f_y(x,y,z,t) = \rho \frac{\partial^2 v}{\partial t^2} \quad (3)$$

where, v is the deformation of the elements in y-direction. By use of plain stress relations [13], the equations can be rewritten as:

$$\begin{cases} \frac{E}{1-\nu^2}\left[\frac{\partial^2 u}{\partial x^2} + \nu \frac{\partial^2 v}{\partial x\, \partial y}\right] - \rho \frac{\partial^2 u}{\partial t^2} = -f_x(x,y,t) \\ \frac{E}{1-\nu^2}\left[\frac{\partial^2 v}{\partial y^2} + \nu \frac{\partial^2 u}{\partial x\, \partial y}\right] - \rho \frac{\partial^2 v}{\partial t^2} = -f_y(x,y,t) \end{cases} \quad (4)$$

where, E is the Young's module and ν is the Poison's ratio.

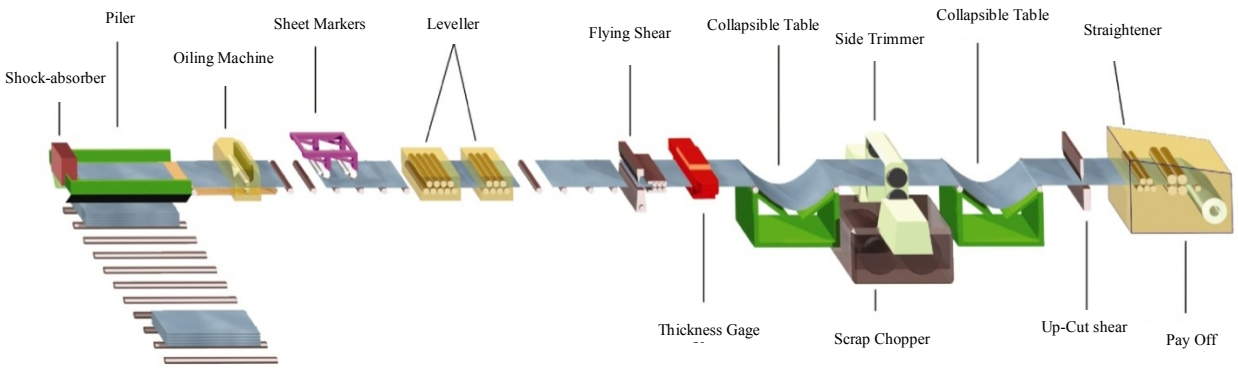

Figure 1. Scheme of heavy-gauge shear line

$$u(x,t) = \begin{cases} F_0\left(\frac{1}{\rho L}\right)T\frac{\pi t + T\sin\left(\frac{-\pi}{T}t\right)}{\pi^2} + \sum_{r=1}^{\infty}\left(\cos\left(\frac{r\pi}{L}x\right)\frac{F_0}{\omega_r}\left(\frac{2}{\rho L}\right)\frac{T}{\pi^2-\omega_r^2T^2}\right. & t < T \\ \left.\left[\pi\sin(\omega_r t) + \omega_r T\ \sin\left(\frac{-\pi}{T}t\right)\right]\right) & \\ F_0\left(\frac{1}{\rho L}\right)T\frac{\pi(2t-T) + T\left(\sin\left(\frac{-\pi}{T}t\right) + \sin\left(\frac{\pi}{T}(T-t)\right)\right)}{\pi^2} + \sum_{r=1}^{\infty}\cos\left(\frac{r\pi}{L}x\right)\frac{F_0}{\omega_r}\left(\frac{2}{\rho L}\right)\frac{T}{\pi^2-\omega_r^2T^2}\times & t \geq T \\ \left[\pi\left(\sin(\omega_r t) + \sin(\omega_r(t-T))\right) + \omega_r T\left(\sin\left(\frac{-\pi}{T}t\right) + \sin\left(\frac{\pi}{T}(T-t)\right)\right)\right] & \end{cases} \quad (8)$$

$$\ddot{u}(x,t) = \begin{cases} -F_0\left(\frac{1}{\rho L}\right)\sin\left(\frac{-\pi}{T}t\right) + \sum_{r=1}^{\infty}\cos\left(\frac{r\pi}{L}x\right)\frac{F_0}{\omega_r}\left(\frac{2}{\rho L}\right)\frac{T}{\pi^2-\omega_r^2T^2}\left[-\pi{\omega_r}^2\sin(\omega_r t) - \omega_r\frac{\pi^2}{T}\sin\left(\frac{-\pi}{T}t\right)\right] & t < T \\ -F_0\left(\frac{1}{\rho L}\right)\left(\sin\left(\frac{-\pi}{T}t\right) + \sin\left(\frac{\pi}{T}(T-t)\right)\right) + \sum_{r=1}^{\infty}\cos\left(\frac{r\pi}{L}x\right)\frac{F_0}{\omega_r}\left(\frac{2}{\rho L}\right)\frac{t_1}{\pi^2-\omega_r^2T^2}\times & \\ \left[-\pi\omega_r^2\left(\sin(\omega_r t) + \sin(\omega_r(t-T))\right) - \omega_r\frac{\pi^2}{T}\left(\sin\left(\frac{-\pi}{T}t\right) + \sin\left(\frac{\pi}{T}(T-t)\right)\right)\right] & t \geq T \end{cases} \quad (11)$$

$$\frac{\ddot{u}(x,t)}{V_0} = \begin{cases} \frac{\pi}{2T}\sin\left(\frac{\pi}{T}t\right) + \sum_{r=1}^{\infty}\cos\left(\frac{r\pi}{L}x\right)\frac{\pi}{r^2\left(\frac{T}{s}\right)^2-1}\left[\frac{r}{s}\sin\left(\frac{r\pi}{s}t\right) + \frac{1}{T}\sin\left(\frac{-\pi}{T}t\right)\right] & t < T \\ \sum_{r=1}^{\infty}\cos\left(\frac{r\pi}{L}x\right)\frac{\pi}{r^2\left(\frac{T}{s}\right)^2-1}\times\left[\frac{r}{s}\left(\sin\left(\frac{r\pi}{s}t\right) + \sin\left(\frac{r\pi}{s}(t-T)\right)\right) + \frac{1}{T}\left(\sin\left(\frac{-\pi}{T}t\right) + \sin\left(\frac{\pi}{T}(T-t)\right)\right)\right] & t \geq T \end{cases} \quad (13)$$

If it is assumed that there is not strain in y-direction and stress variations are negligible in this direction, it would be possible to replace Equation (4) with Equation (5).

$$\frac{E}{1-\nu^2}\left[\frac{\partial^2 u}{\partial x^2}\right] - \rho\frac{\partial^2 u}{\partial t^2} = -f_x(x,t) \quad (5)$$

The contact force is the only force that is applied to the front edge of the plate (head of the plate) during the contact duration. Here, it is assumed that the contact force has a half-sine behavior which is introduced by Equation (6) and is shown in Figure 4.

$$f(x,t) = F_0\delta(x)1(t)\sin\left(\frac{\pi}{T}(t)\right) - F_0\delta(x)1(t-T)\sin\left(\frac{\pi}{T}(t-T)\right) \quad (6)$$

where, F_0 is the maximum amount of the force, T is the contact period, $\delta(x)$ is the impulse function, and 1(t) is the unit step function. By plugging Equation (6) to (5), it is possible to solve the equation of motion. The separation of variables method suggests that the solution of Equation (5) has the following form.

$$u(x,t) = U(x)\,G(t) \quad (7)$$

The solution is attained through the following relation, using the modal analysis and the convolution integral [14] in order to calculate $U(x)$ and $G(t)$, respectively.

In Equation (8), L is the length of the plate, and ω_r and c are identified as the natural frequency of longitudinal vibration and the speed of longitudinal elastic waves in the plate, respectively. The quantities are given by Equations (9) and (10).

$$\omega_r = \frac{r\pi}{L}c \quad (9)$$

$$c = \sqrt{\frac{E}{\rho(1-\nu^2)}} \quad (10)$$

Based on the Raleigh integral and monopole equation, the only term that generates the sound is the acceleration. Consequently, Equation (8) was differentiated to obtain the plate acceleration. The Equation (11) shows the derivation.

The plate should be laid off after the impact; consequently, by integrating the contact force through the contact duration and using the momentum law, the following relation is established for contact force behavior:

$$F_0 = \frac{\pi L\rho V_0}{2T} \quad (12)$$

where, V_0 is the initial velocity of the plate. By plugging this equation into Equation (11), the longitudinal acceleration will be as Equation (13); where, s is the time that elastic wave needs to pass through the length of the plate. This time is calculated as follows.

$$s = \frac{L}{c} \quad (14)$$

Equation (13) is then used to determine the sound generated by head and tail of the plate. The surface acceleration in direction of normal to the surfaces is the only element which partakes in the sound creation. In order to determine the radiated sound from the top and the bottom surfaces of the plate, the accelerations of both the surfaces in z-direction is necessary. To specify these accelerations, it is possible to use plain-stress relations for the plate as following [13]:

$$\varepsilon_z = -\nu(1+\nu)\varepsilon_x \quad (15)$$

$$w(x,t) = \frac{h}{2}\varepsilon_z \quad (16)$$

where, ε_x is the strain in x-direction, ε_z is the strain in z-direction, w is the deformation of the surfaces of plate in

z-direction, and h is the thickness of the plate. The following equation is also available for the strain.

$$\varepsilon_x = \frac{\partial u}{\partial x} \tag{17}$$

Therefore, the strain in x-direction is calculated by differentiating Equation (8). This predicted strain and Equation (15) are then used in Equation (16) to calculate the deformation of the surfaces as attained in follows Equation (18).Finally, the acceleration of the surfaces of the plate in z-direction is obtained as following Equation (19). A comparison between Equations (13) and (19) shows that the behavior of $\ddot{w}$ is partly similar to $\ddot{u}$, while the order of $\ddot{w}$ is about $\frac{\pi}{L}\frac{h}{2}\nu(1+\nu)$ times less than $\ddot{u}$. Figure 5 shows the surface acceleration for a steel plate with a length of one meter, width of 0.6 m, and the thickness of 3 millimeter which impacts to a shock-absorber with initial velocity of 2 m/s. The contact duration for the collision is assumed to be one millisecond. The previous result and the Figure 5 shows that the acceleration of the edges is much more than that of the surfaces Therefore, the edges of the plate have more significant role in noise creation compared to the surfaces of the plate. This fact is more clarified in section 3.

It was mentioned that the radiated sound was related to the surface acceleration. Therefore, the pick of the radiated noise was related to the pick of the accelerations. It was also declared that the behavior of $\ddot{w}$ was similar to $\ddot{u}$ and was shown that $\ddot{u}$ had more significant affect in the noise generation. Accordingly, the pick of $\ddot{u}$ in the head and tail edges of the plate has almost direct relation with the pick of the generated sound. Here, the pick of $\ddot{u}$ in the head and tail edges is surveyed to estimate the behavior of the sound pick.

By plugging in x equal zero in Equation (13), it is apparent that the maximum acceleration is a function of V_0, T, and s. If these variables are replaced by numerical amounts, the acceleration pick, $\ddot{u}_{max}$ is calculated (see Figure 6). This figure shows the acceleration pick for different amount of T and s. Each curve of the figure shows the variation of acceleration pick for an amount of s. The dash-line curve plotted in the figure correlates to the acceleration of the rigid body motion. This curve is produced by dividing the contact force to the mass of the plate which is 14 kg. Denoted points in this figure are related to the minimum amount of the conceivable contact duration. When the plate collides with a rigid wall, the contact duration reaches to the minimum level. Here, the contact duration is equal to $2L/c$ [15].

$$w(x,t) = \begin{cases} -\frac{h}{2}\nu(1+\nu)\sum_{r=1}^{\infty}\left(\frac{-r\pi}{L}\right)sin\left(\frac{r\pi}{L}x\right)\frac{F_0}{\omega_r}\left(\frac{2}{\rho L}\right)\frac{T}{\pi^2-\omega_r^2T^2}\left[\pi sin(\omega_r t)+\omega_r T sin\left(\frac{-\pi}{T}t\right)\right] & t<T \\ -\frac{h}{2}\nu(1+\nu)\sum_{r=1}^{\infty}\left(\frac{-r\pi}{L}\right)sin\left(\frac{r\pi}{L}x\right)\frac{F_0}{\omega_r}\left(\frac{2}{\rho L}\right)\frac{T}{\pi^2-\omega_r^2T^2}\times & t\geq T \\ \left[\pi\left(sin(\omega_r t)+sin(\omega_r(t-T))\right)+\omega_r T\left(sin\left(\frac{-\pi}{T}t\right)+sin\left(\frac{\pi}{T}(T-t)\right)\right)\right] & \end{cases} \tag{18}$$

$$\frac{\ddot{w}(x,t)}{V_0} = \begin{cases} \frac{\pi}{L}\frac{h}{2}\nu(1+\nu)\sum_{r=1}^{\infty}r.sin\left(\frac{r\pi}{L}x\right)\frac{\pi}{r^2\left(\frac{T}{s}\right)^2-1}\left[\frac{r}{s}sin\left(\frac{r\pi}{s}t\right)+\frac{1}{T}sin\left(\frac{-\pi}{T}t\right)\right] & t<T \\ \frac{\pi}{L}\frac{h}{2}\nu(1+\nu)\sum_{r=1}^{\infty}r.sin\left(\frac{r\pi}{L}x\right)\frac{\pi}{r^2\left(\frac{T}{s}\right)^2-1}\times & t\geq T \\ \left[\frac{r}{s}\left(sin\left(\frac{r\pi}{s}t\right)+sin\left(\frac{r\pi}{s}(t-T)\right)\right)+\frac{1}{T}\left(sin\left(\frac{-\pi}{T}t\right)+sin\left(\frac{\pi}{T}(T-t)\right)\right)\right] & \end{cases} \tag{19}$$

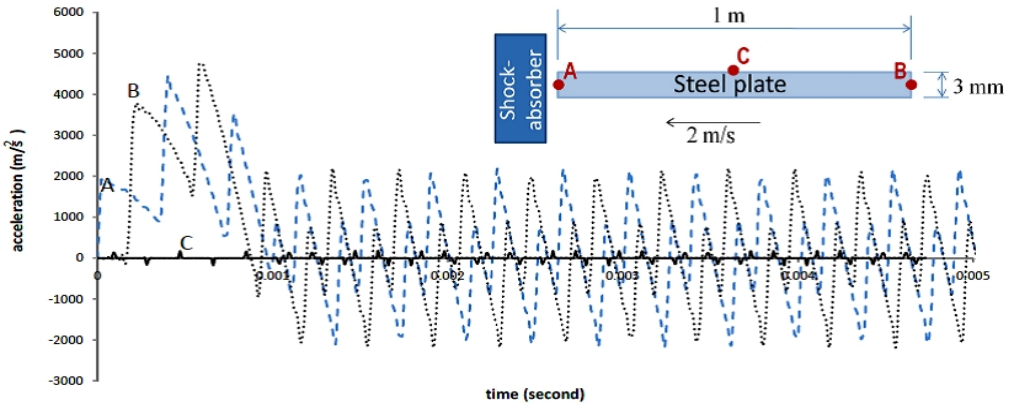

Figure 5. Surface acceleration in different points of the plate

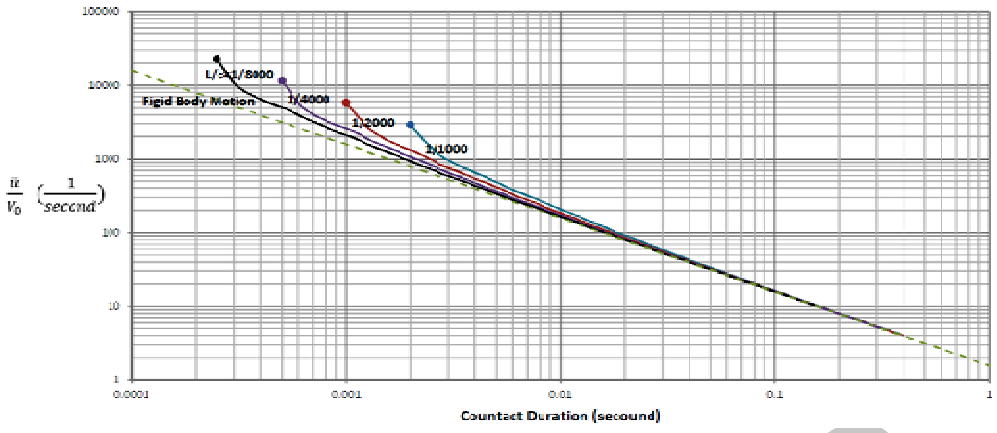

Figure 6. Acceleration pick in x-direction for the head of the plate

Figure 6 Shows that when contact duration is low, the analytical curves deviate from rigid body motion line. Consequently, the contribution of modal vibration in generated acceleration is increased. However, the acceleration pick can be estimated by the rigid body motion acceleration if the contact duration is increased.

Based on the figure, in order to make the estimation error less than 10 percent, the contact duration must be 16 times greater than the minimum feasible contact duration. The comparison between the denoted points and the dash-line curve shows that if the contact duration is close to the minimum level, the estimated acceleration pick is 3.5 times less than that for the actual amount.

3. SOUND GENERATIO

As expressed before, the surfaces of the plate are partitioned in two parts for sound estimation. The noise from each part is estimated separately and the obtained results are superposed together. In the previous section, it was assumed that the strain in z-direction is negligible; therefore, the sides of the plate do not generate any sound. Head and tail of the plate have a very fine thickness; subsequently, if these edges are divided to a number of elements, each element radiate could be assumed as a monopole. The sensed acoustic pressure at the time t that is generated by a monopole in a position with distance of r from the monopole is [16]:

$$P(r,t) = \frac{\rho_{air}}{4\pi r}\dot{Q}\left(t-\frac{r}{c_{air}}\right) \quad (20)$$

where, ρ_{air} and c_{air} are density and sound speed in the air, respectively. Q is the volume velocity which is defined as volume of the air that is replaced by the sound source motion. Hence, the $\dot{Q}$ for the head and tail of the plate presented as:

$$\dot{Q}\left(t-\frac{r}{c}\right) = -h\ \ddot{u}\left(t-\frac{r}{c}\right)\Big|_{x=0}$$
$$\dot{Q}\left(t-\frac{r}{c}\right) = h\ \ddot{u}\left(t-\frac{r}{c}\right)\Big|_{x=L} \quad (21)$$

The generated sound by the head and tail edges of the plate is evaluated by plugging Equation (21) into (20) and integrating through the width of the plate.

Top and bottom surfaces of the plate are flat and extended. Thus, the Rayleigh integral equation is used to determine generated acoustic pressure with these surfaces [17]. The sensed acoustic pressure in a position with coordinates of X, Y, and, Z are evaluated by the following equation:

$$P(X,Y,Z,t) = \frac{\rho_{air}}{2\pi}\iint \frac{\ddot{w}\left(x,y,z,t-\frac{d}{c_{air}}\right)}{d}ds \quad (22)$$

where, ds is an element of the surface and d is the distance between the element and the given position. Gaussian integration can be employed to determine integrations of Equations (20) and (22). The acoustic pressure that is evaluated by the use of each equation is demonstrated in Figure 7 for a position with distance of 0.2 m from the head of the plate with the assumed dimension shown in Figure 5.

As shown in Figure 7, the generated sound by the surfaces of the plate is 100 times less than the generated sound by the edges of the plate. Therefore, it is clear that the sound generally is radiated by the edges of the plate rather than the surfaces. This fact confirms that the Figure 6 introduces a good criterion to study the sensitivity of the sound intensity to different parameters involved in such a problem.

When a plate with free boundary condition is impacted longitudinally, it can just buckle by principle mode of bending vibration [18]. As a result, acoustic waves which are created by the buckling have the frequency of principle mode. The principle natural frequency of the plate is 15.6 Hz.

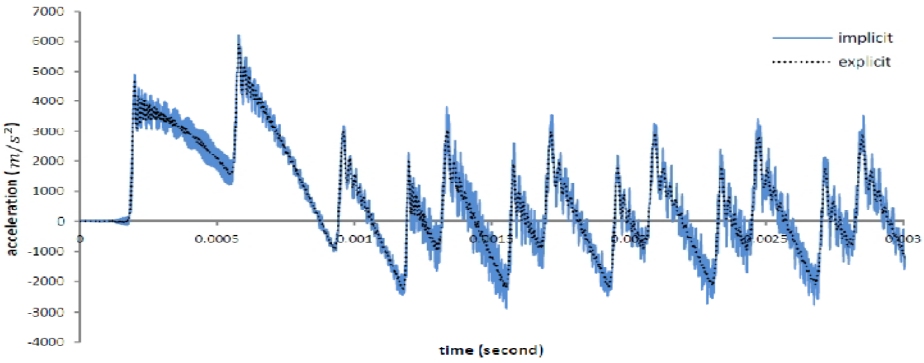

Figure 8. Longitudinal acceleration for the head of the plate

This value indicates that the frequency of the created sound by buckling is not in the audible range. Regarding to A-scale weighting factor, it is clear that the frequency does not have any persecutor effect in human auditory system, even though the frequency of principle mode is in audible range. Consequently, the effect of the buckling on the noise generation is not studied.

4. FINITE ELEMENT ANALYSIS

In the last section, the generated sound around the plate is estimated. Here, the same can be calculated by use of finite element method (FEM). The FEM results can show the abilities and limitations of the method in order to simulate the acoustic phenomena.

The problem was simulated uncoupled to reduce the computational cost. Therefore, first the plate was simulated and excited by a half-sine force and then the state variables of the plate which were caused by the applied force were obtained. Using the state variables, the air in the environs of the plate was exited to obtain the acoustic field.

4. 1. The Plate Simulation Using the virtual work equation and neglecting the structural damping, the FEM equation can be written as [19]:

$$M^{NM}\ddot{u}^{M} + I^{N} - P^{N} = 0 \quad (23)$$

where, M^{NM} is the mass matrix, I^{N} is the internal force vector, and P^{N} represents the external force vectors that are calculated as follows:

$$M^{NM} = \int_{V} \rho N^{N}.N^{M} dV \quad (24)$$

$$I^{N} = \int_{V} \beta^{N}:\boldsymbol{\sigma}\, dV \quad (25)$$

$$P^{N} = \int_{S} N^{N}.\mathbf{t}\, dS + \int_{V} N^{N}.\mathbf{F}\, dV \quad (26)$$

In the above equations N^{N} is the displacement interpolator function, β^{N} is the strain interpolator function, $\boldsymbol{\sigma}$ is the stress tensor, $\mathbf{t}$ is the surface tractions, and $\mathbf{F}$ shows the body forces. Equation (23) is solved explicitly and implicitly. By studying mesh sensitivity, it is revealed that the use of 1cm elements is appropriate for plate simulation. The Equation (23) is solved through discretizing the plate by the 1cm and 8 node linear elements. Figure 8 shows the longitudinal acceleration of the plate head

Figure 8 shows that some noises exist in the obtained explicit and implicit curves. These noises in the explicit method are less than that of the implicit method. On the other hand, by applying the same time increments for both methods it is seen that the implicit calculation time is 100 times more than that of the explicit method. Therefore, the explicit method is more appropriate in solving the given problem. Figure 9 shows the conformity of FEM results compared with the analytical results.

Figure 9 shows that the FEM curve is swayed around the analytical curve, while, it should be said that these perturbations in FEM curve are created by the post-processor computations and have a frequency higher than the audible range. Therefore, it looks like that the perturbations do not affect the estimation of sound and do not make any error in FEM acoustic simulations.

4. 2. The Air Simulation Generally, the surface velocities and the surface accelerations are the two objects that excite the air and generate the acoustic waves. However, in the great majority of practical applications, the acoustic tractions associated with the volumetric drag are negligible compared to those associated with the fluid inertia, so that this term is ignored in transient analysis. In this condition, the effects of surface velocity are ignored. Therefore, it is assumed that the acceleration of surfaces is the only

factor which excites the air. By studying the equilibrium equation for a small element of the air and neglecting the volumetric drag, the acoustical FEM formulation for the problem would be written as [20]:

$$M_f^{PQ}\ddot{p}^Q + C_{fr}^{PQ}\dot{p}^Q + \left(K_f^{PQ} + K_{fi}^{PQ}\right)p^Q - S_{fs}^{PM}\ddot{u}^M = 0 \quad (27)$$

where,

$$M_f^{PQ} = \int_{V_f} \frac{1}{K_f} H^P H^P dV \quad (28)$$

$$C_{fr}^{PQ} = \int_{S_{fi}} \frac{1}{c_1} H^P H^P dS \quad (29)$$

$$K_f^{PQ} = \int_{V_f} \frac{1}{\rho_f} \frac{\partial H^P}{\partial \mathbf{x}} \cdot \frac{\partial H^Q}{\partial \mathbf{x}} dV \quad (30)$$

$$K_{fi}^{PQ} = \int_{S_{fi}} \frac{1}{a_1} H^P H^P dS \quad (31)$$

$$S_{fs}^{PM} = \int_{S_{fs}} H^P \mathbf{n} \cdot N^M dS \quad (32)$$

In the above equations, p is the acoustic pressure, $\ddot{u}$ is the surface acceleration, H^P is the pressure interpolator, N^M is the displacement interpolator, K_f and ρ_f are the bulk modulus and density of the air, respectively, V_f is the volume of the air, S_{fs} is the interface of the air and plate, $\mathbf{n}$ is the normal vector of the surface, and S_{fi} is the radiated boundary.

The radiated boundary in the external problem is used to simulate the exterior surface of the finite elements as this surface shows the behavior of the extreme area. Other parameters of a planar radiated surface are calculated as follows:

$$\frac{1}{c_1} = \frac{1}{\sqrt{\rho_f K_f}} \quad (33)$$

$$\frac{1}{a_1} = \frac{\gamma}{2\rho_f \sqrt{\rho_f K_f}} \quad (34)$$

By plugging the obtained surface accelerations into Equation (27), the pressure field around the plate was calculated. In the external acoustical problem, two constraints have to be observed in order to obtain adequate FEM results. First, the distance of the radiated boundary with acoustic sources (standoff thickness) must be as great as possible. Second, the mesh size must be as small as possible. Some of the references [19, 21] give some criterion about these constraints. For example, ABAQUS suggests that the standoff thickness must be 1/3 times greater than that of the acoustical wavelengths maximum and the biggest element in the mesh must be 10 times smaller than that of the acoustical wavelengths minimum.

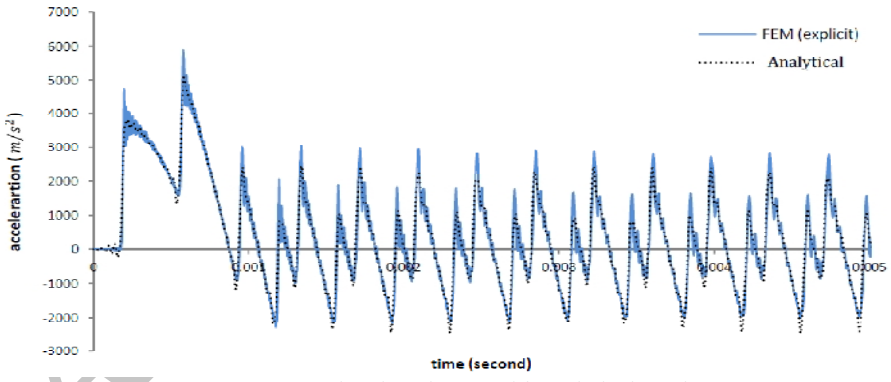

Figure 9. Conformity of FEM with analytical results

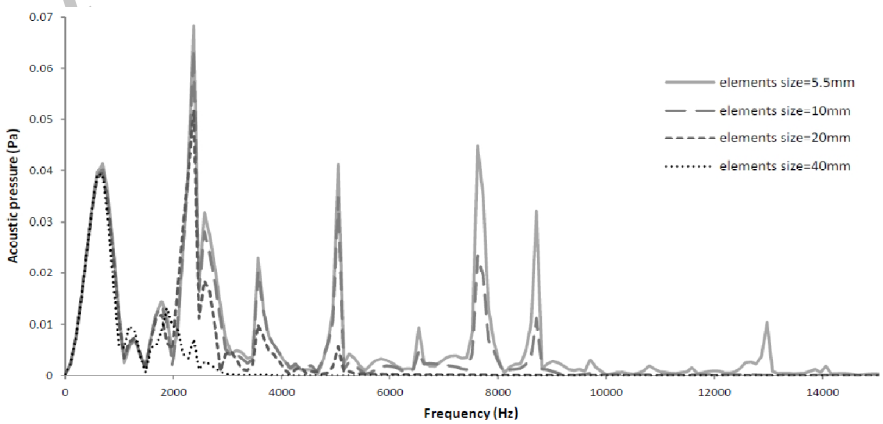

Figure 10. Acoustic pressure spectra that is obtained by different mesh sizes.

Based on these criterions, it is clear that the small elements should be used to simulate high frequency and large standoff thickness to simulate low frequency. Consequently, these constraints must be considered to generate adequate mesh. Figure10 shows the fast Fourier transform (FFT) of FEM results. Each curve in this figure is gained by a specific mesh size. The linear elements with 8 nodes were used to discrete the acoustic medium. The standoff thickness in all of these meshes was 20 centimeters. Increasing the interest frequency, the smaller elements have to be used in order to obtain appropriate results. Considering these four frequencies in the last figure: 0.79kHz, 2.4kHz, 5.0kHz, and 7.6kHz, Figure 11 illustrates the mesh convergence for these frequencies. Figure 11 shows that in all of these frequencies, the FEM results will be converged using 5.5mm elements. Therefore, it is assumed that the gained result by the element size is the most accurate ones. Based on this assumption, the error of prediction of sound intensity in different frequencies using different mesh sizes is calculated. Figure 12 shows the percentage of error for each mesh in comparison with the results gained using 5.5mm elements. Figure 12 illustrate that if 10 mm elements are used, one can just simulate frequency less than 4kHz that have less than 10% error. It is clear that if 20 mm elements are used, only the frequencies less than 1.2 kHz would have the same error of simulation. As a result, in spite of the previous researches that give a linear criterion between the wavelength and the size of the elements, it is obvious that this relation is not linear. Figure 12 can be represented in another form as Figure 13.

Figure 13 can tribute to the selection of proper element for this simulation. The figure shows that the previous criteria are not for all of the frequencies. For instance, for frequencies 700 and 7000 Hz, the size of the elements must be 12.5 and 7.5 times less than the wavelength of the waves, respectively for securing less than 10% error. Consequently, it is suggested that Equation (35) be applied to improve the size of the elements and interest wavelength ratio.

$$r = 13 - 0.9f \quad (35)$$

In this equation f shows the interest frequency (kHz) and r is the element size and the wavelength ratio. This equation is useable just for frequencies lower than 7 kHz. For frequencies higher than 7 kHz, the ratio of 6 should be used.

The standoff thickness is an effective parameter in FEM simulation. Figure 14 shows the FFT of FEM results for different meshes. Each curve of the figure is obtained by a separate mesh with different standoff thickness. The standoff thickness affects the waves with the great wavelength or low frequency. Therefore, in this study only the effect of standoff thickness on the low frequency range is of concern. For this purpose, linear element with 8 nodes and 2cm length is applied here. The element is appropriate only for the frequencies lower than 1.5 kHz, based on the last criterion. Figure 14 shows that the simulations have to be performed with the standoff thickness of more than 0.5 m in order to obtain an accurate result for this range of frequency. By applying the previous explanations, a space of the air is modeled with 0.5 m stand of thickness and the medium is meshed with 1cm linear elements. Figure15 shows the result of this modeling. Analytical curve that is obtained in section 3 is also plotted here. The comparison between these two curves shows the accuracy of the FEM solution. The differences in these two curves are caused by the numerical errors and the assumptions made in section 3. For instance, it was assumed that the top and bottom surfaces of the plate are extremely extended in the air and each element of the plate edges radiates as a monopole.

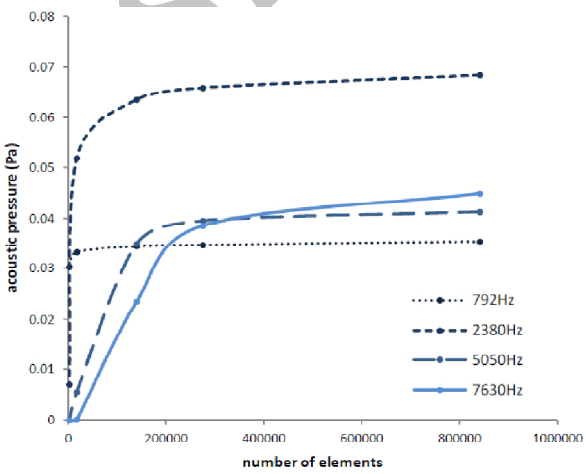

Figure 11. Mesh convergence for different frequencies

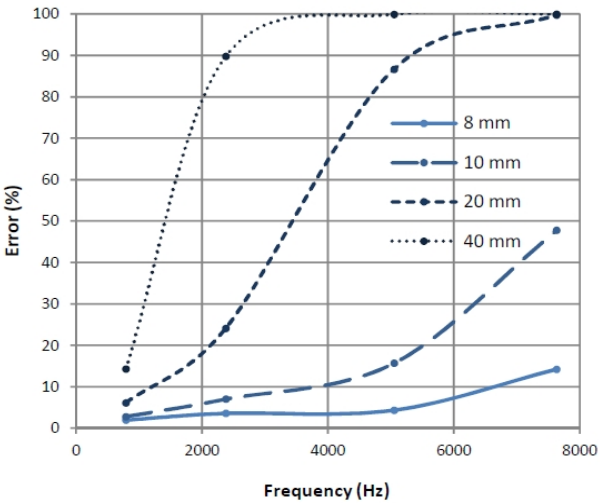

Figure 12. Error of each meshing to estimate sound intensity in different frequencies

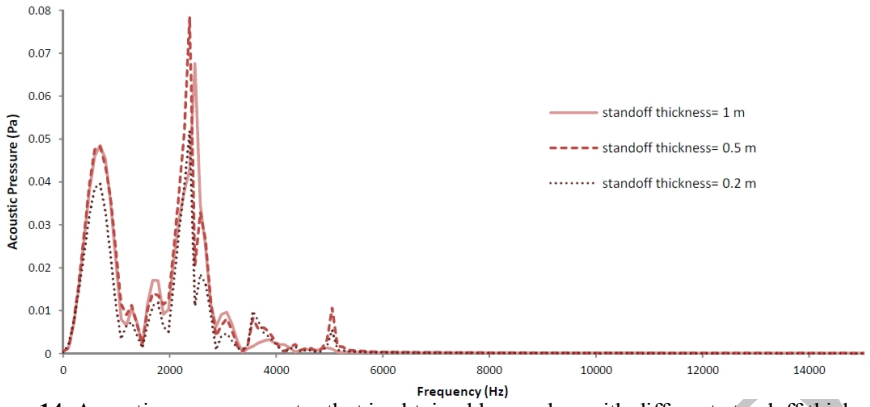

Figure 14. Acoustic pressure spectra that is obtained by meshes with different standoff thickness.

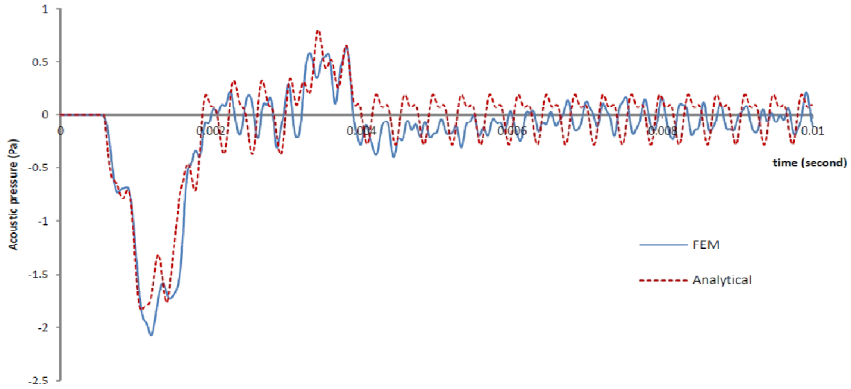

Figure 15. Sensed Acoustic pressure in point A for different times

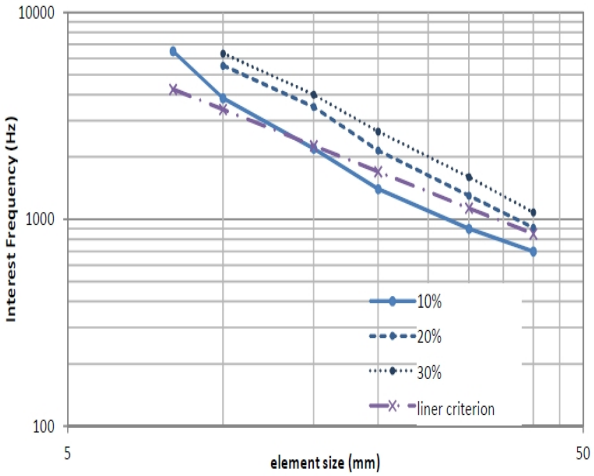

Figure 13. Suitable element size in proportion with interest frequency and interest precision

5. CONCLUSION

The generated sound by a steel plate which is impacted in a longitudinal manner was studied. The noises are generally created by the head and tail edges of the plate. Although the sound is created by these edges, it does not mean that the sound is merely generated by the rigid body motion, at all. The difference between the plate acceleration pick and the rigid body motion acceleration shows the contribution of modal vibration in sound generation. This article provides some good criteria to help scholars in academia and industry find out more about the sensitivity of the sound intensity to different parameters and optimize the plate shock-absorbers. It was shown that the pick of the edges acceleration can be estimated by rigid body acceleration. If the contact period is 32 times greater than the time needed for the longitudinal waves to pass through the plate, the error of this estimation will be less than 10 percent. By decreasing the contact duration, the error in the estimation is raised. In the worst condition, the estimation is 3.5 times less than the actual amount of acceleration pick. Choosing an appropriate element is very crucial in the acoustic simulations. Some researchers have introduced a constant ratio to select appropriate size for acoustic elements by considering the sound wavelengths. FEM simulations in this research showed that use of a constant ratio for all of the frequencies in audible range is not proper. The ratio is greater for the low frequency waves and is lower for the high frequency waves. Based on this fact, a new ratio was introduced which was sensitive to the waves

frequencies. In acoustic simulation, it is possible that an extensive frequency range is considered significance. Results showed that the acoustic meshes were very sensitive to the interest frequencies. Therefore, available waves in the problem and their frequencies should be distinguished. It should be specified that, which of these waves are significant and should undergo more studies. Otherwise, one has to mesh a broad space with very fine acoustic elements. This causes huge computational cost which may make the problem at hand unsolvable.

6. REFERENCES

1. Nishimura, G. and Takahashi, K., "Impact sound by mutual collision of two steel balls", ***Bulletin of the Japan Society of Precision Engineers***, Vol. 1, (1965), 47-51.
2. Koss, L. and Alfredson, R., "Transient sound radiated by spheres undergoing an elastic collision", ***Journal of Sound and Vibration***, Vol. 27, No. 1, (1973), 59-75.
3. Yufang, W. and Zhongfang, T., "Sound radiated from the impact of two cylinders", ***Journal of Sound and Vibration***, Vol. 159, No. 2, (1992), 295-303.
4. Richards, E., Carr, I. and Westcott, M., "On the prediction of impact noise, v: The noise from drop hammers", ***Journal of Sound and Vibration***, Vol. 88, No. 3, (1983), 333-367.
5. Akay, A., Bengisu, M. and Latcha, M., "Transient acoustic radiation from impacted beam-like structures", ***Journal of Sound and Vibration***, Vol. 91, No. 1, (1983), 135-145.
6. Wåhlin, A., Gren, P. and Molin, N. E., "On structure-borne sound: Experiments showing the initial transient acoustic wave field generated by an impacted plate", ***The Journal of the Acoustical Society of America***, Vol. 96, (1994), 2791.
7. Schedin, S., Lambourg, C. and Chaigne, A., "Transient sound fields from impacted plates: Comparison between numerical simulations and experiments", ***Journal of Sound and Vibration***, Vol. 221, No. 3, (1999), 471-490.
8. Ross, A. and Ostiguy, G., "Propagation of the initial transient noise from an impacted plate", ***Journal of Sound and Vibration***, Vol. 301, No. 1, (2007), 28-42.
9. Akay, A. and Latcha, M., "Sound radiation from an impact-excited clamped circular plate in an infinite baffle", ***The Journal of the Acoustical Society of America***, Vol. 74, (1983), 640.
10. Sakagami, K., Michishita, K., Morimoto, M. and Kitamura, Y., "Sound radiation from a baffled elastic plate strip of infinite length with various concentrated excitation forces", ***Applied Acoustics***, Vol. 55, No. 3, (1998), 181-202.
11. Putra, A. and Thompson, D., "Sound radiation from rectangular baffled and unbaffled plates", ***Applied Acoustics***, Vol. 71, No. 12, (2010), 1113-1125.
12. Tao, J., Liu, G. and Lam, K., "Sound radiation of a thin infinite plate in light and heavy fluids subject to multi-point excitation", ***Applied Acoustics***, Vol. 62, No. 5, (2001), 573-587.
13. Sadd, M. H., "Elasticity: Theory, applications, and numerics", Access Online via Elsevier, (2009).
14. Hagedorn, P., "Vibration and waves in continuous mechanical systems", USA, John Wiley & Sons, (2007).
15. Goldsmith, W., "Impact, the theory and physical behavior of colliding solids", (1964).
16. Kuttruff, H., "Acoustics", Taylor & Francis, USA, (2007).
17. Strutt, J. W., Rayleigh, B. and Lindsay, R. B., "The theory of sound", Dover New York, Vol. 1, (1945).
18. Cui, S., Hao, H. and Cheong, H. K., "Numerical analysis of dynamic buckling of rectangular plates subjected to intermediate-velocity impact", ***International Journal of Impact engineering***, Vol. 25, No. 2, (2001), 147-167.
19. Simulia, D. S., "ABAQUS theory manual" (2009), Version.
20. Ihlenburg, F., "Finite element analysis of acoustic scattering", Springer, Vol. 132, (1998).
21. Łodygowski, T. and Sumelka, W., "Limitations in application of finite element method in acoustic numerical simulation", ***Journal of Theoretical and Applied Mechanics***, Vol. 44, No. 4, (2006), 849-865.

Numerical and Analytical Investigation in Radiated Noise by a Shock-Absorber

K. Mehraby[a], H. Beheshti[b], M. Poursina[b]

[a] *Department of Mechanical Engineering, University of Shahrekord, Sharekord, Iran*
[b] *Department of Mechanical Engineering, University of Isfahan, Isfahan, Iran*

PAPER INFO

Paper history:
Received 07 October 2012
Accepted in revised form 16 May 2013

Keywords:
Noise
Impact
Shock-Absorber
Acoustics

چکیده

در این تحقیق چگونگی انتشار صدا از یک ضربه گیر صنعتی مورد مطالعه قرار خواهد گرفت. این ضربه‌گیر در خط برش سنگین ورق‌های فولادی به منظور متوقف نمودن آنها مورد استفاده قرار می‌گیرد. برای محاسبه میزان صدای انتشار یافته به محیط به صورت تئوری سه گام برداشته خواهد شد. در گام اول پاسخ ارتعاشی ورق در اثر برخورد صورت گرفته تعیین می-گردد. در گام دوم با جای گذاری مجموعه‌ای از تک قطبی‌ها در لبه‌های ورق صدای ایجاد شده از لبه‌ها تخمین زده شده و در نهایت در گام سوم به منظور پیشبینی صدای انتشار یافته از سطوح ورق معادله انتگرال ریلی مورد استفاده قرار می‌گیرد. همچنین در این مطالعه برای حل این مسئله روش المان محدود به کار گرفته شده تا ضمن مقایسه نتایج حاصل از دو روش شناخت کاملتری از چگونگی انتشار صدا ایجاد گردد.

doi: *10.5829/idosi.ije.2013.26.12c.13*